Chapter 8
Groundwater Temperature

Abstract Changes of temperature in response to earthquakes have long been documented and, in the case where systematic patterns of change can be discerned, may reveal important hydrogeologic processes. Progress in our understanding of these processes, however, has been slow, largely because systematic measurements are relatively scarce. In this chapter we review some cases where earthquake-induced changes of groundwater temperature were documented and interpreted. More importantly, we show that most interpretations are under-constrained and accurate explanation of the measured changes is often difficult. In order to better constrain the interpretation, co-located measurement of groundwater flow from conductive fractures or formations intersecting the wells is needed to interpret temperature measurements. An often neglected mechanism is turbulent mixing of water in wells, which may occur frequently during earthquakes because the water column in a well at thermal equilibrium with the local geotherm is usually in a state of mechanical disequilibrium.

8.1 Introduction

Changes of temperature in response to earthquakes have been documented in many wells over the past several decades (e.g., Ma et al. 1990). Such changes may be expected, not only because earthquake-induced groundwater flow is effective in transporting heat, but because significant amounts of frictional heat could be generated along the ruptured fault, which may raise groundwater temperature. Progress in our understanding of these processes, however, has been slow, largely because relevant quantitative data are relatively scarce. Instrumental measurements of earthquake-induced temperature changes started in the late twentieth century and continuous recording of temperature has only become recently available. In the next section (Sect. 8.2), we review some recent studies of groundwater temperature responses to earthquakes, starting with the response to the 2008 Mw7.9 Wenchuan earthquake across the Chinese continent (He and Singh 2020), followed by the response to the 2016 Mw7.0 Kumamoto earthquake in central Kyushu, Japan (Miyakoshi et al.

C. Wang and M. Manga, *Water and Earthquakes*,
Lecture Notes in Earth System Sciences,
https://doi.org/10.1007/978-3-030-64308-9_8

2020), and ending with the response to the 2016 Mw5.8 Gyeongju earthquake in a well in SW South Korea (Lee et al. 2020).

While the earthquake-induced changes of groundwater temperature may be difficult to interpret in general, systematic patterns of the changes may be discerned and interpretation of the patterns may be made if the flow and the geometry of the drainage basin is relatively simple, the hydrogeology understood, and the data abundant. We devote Sect. 8.3 to discuss how regional patterns in these changes may be discerned and interpreted to better understand earthquake-related hydrogeological processes.

In Sect. 8.4 we review the studies of temperature changes in springs during earthquakes. One such study focuses on some cold springs in central Kyushu, Japan, before and after the 2016 Mw7.9 Kumamoto earthquake, Japan. The other case is a classic study of temperature changes in a hot springs in central Honshu in response to remote earthquakes (Mogi et al. 1989).

In Sect. 8.5 we review studies of temperature changes beneath the seafloor. One is the study of the temperature change on a ruptured fault beneath the Japan Trench, which ruptured during the 2011 Mw9.0 Tohoku-Oki earthquake off the Pacific coast of Japan (Fulton et al. 2013; Fulton and Brodsky 2016). The others are temperature measurements near the Juan de Fuca ridge off the Pacific coast of western US (Johnson et al. 2000; Davis et al. 2001; Dziak et al. 2003).

An important ambiguity in our understanding of earthquake-induced change of groundwater temperature originates from the uncertainty in the interpretation of the groundwater data. Most interpretations of such changes (e.g., He and Singh 2020; Miyakoshi et al. 2020; Lee et al. 2020) invoke the mechanism of enhanced permeability during earthquakes (e.g., Manga et al. 2012). A less well known, but potentially common, occurrence is the turbulent mixing of water in wellbores (Shi et al. 2007), which has become increasingly invoked in debates about the mechanisms of groundwater temperature change during earthquakes (e.g., Sections 8.2.3, 8.5.1, 8.5.2). We discuss this occurrence together with its observational and physical basis in Sect. 8.6. We also make recommendations in the concluding remarks for future research on earthquake-induced temperature changes.

8.2 Land Measurements

8.2.1 China

A comprehensive study was made of the response of groundwater temperature over the Chinese continent to the 2008 Mw7.9 Wenchuan earthquake, during which the groundwater temperature in numerous wells on the Chinese mainland showed changes (He and Singh 2020). Figure 8.1a shows that the spatial distribution of the coseismic change of groundwater temperature is random and does not correlate with the focal mechanism of the Wenchuan earthquake (shown by the beach-ball symbol) or the epicentral distance. Figure 8.1b shows that the response of water level to the

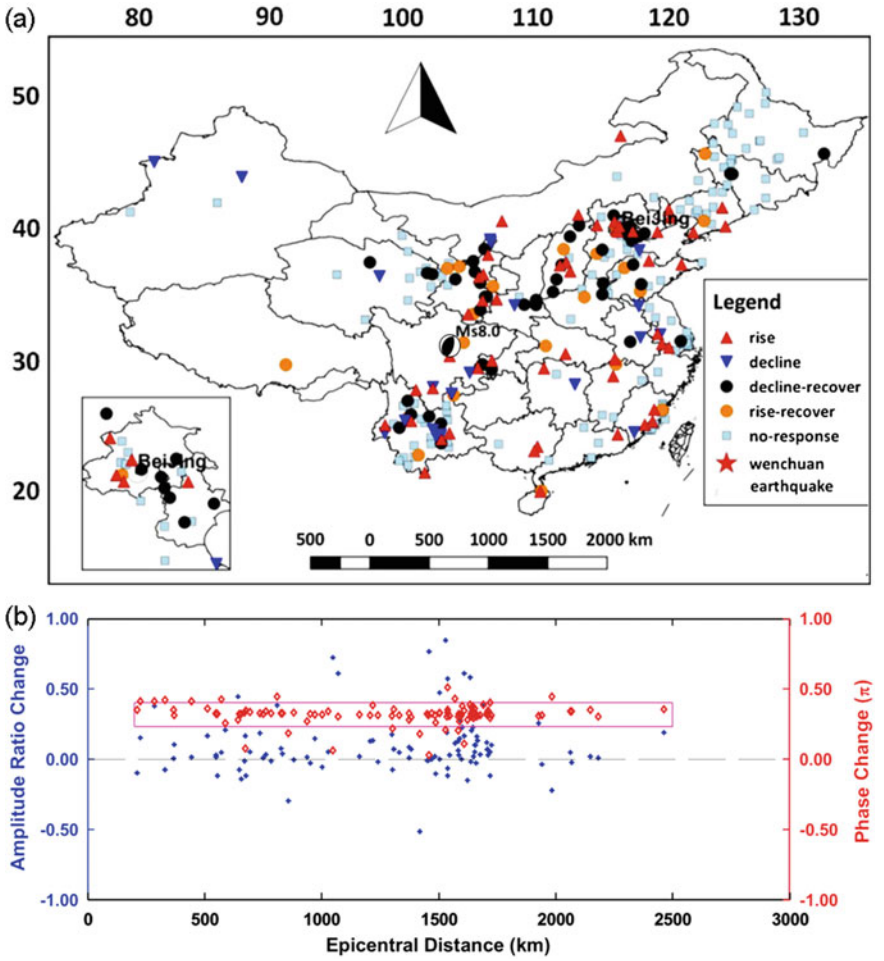

Fig. 8.1 **a** Spatial distribution of groundwater measurement wells in mainland China. Beach ball symbol shows the epicenter and the focal mechanism of the 2008 Wenchuan earthquake. The red triangles denote locations of coseismic rise of groundwater temperature, the inverted dark blue triangles denote coseismic decline of groundwater temperature, the black circles denote a coseismic decline followed by recovery, the yellow circles represent a coseismic rise followed by recovery, and the light blue squares indicate no change of the groundwater temperature. The inset window shows the spatial distribution of monitoring wells around Beijing. (from He and Singh 2020). **b** Changes of phase (red symbols, in unit of π) and amplitude ratio (blue symbols) of water level response to the M2 tide in the studied wells after the Wenchuan earthquake. Positive changes correspond to phase advance and amplitude increase, respectively (from He and Singh 2019)

M2 tide in these wells show a nearly uniform phase advance and a random change of amplitude ratio (He and Singh 2019). The phase advance of the tidal response of groundwater level after the Wenchuan earthquake (Fig. 8.1b) suggests a coseismic enhancement of the permeability in all the studied aquifers (see Chap. 5, Sect. 5.4), which in turn suggests an enhanced coseismic exchange of groundwater between the aquifer and the well. Because the relative location between the temperature gauge and the hydraulically conductive fractures/formations that intersect the well is unknown in most wells, and because the relative location may control the coseismic temperature change as explained later, the coseismic changes of groundwater temperature appear spatially random and disordered, as noted by the authors.

He and Singh (2020) identified four types of temperature changes (Fig. 8.2), i.e., sustained temperature rise after the earthquake, sustained temperature fall after the earthquake, transient coseismic fall that was followed shortly afterwards by recovery, and transient coseismic rise that was followed shortly afterwards by recovery. Here we group these responses into two categories: sustained temperature changes that continue for more than 10 days (Fig. 8.2a, b), and transient temperature changes (either transient rises or transient falls) that recover within a day (Fig. 8.2c, d). As we discuss later, these two categories of earthquake-induced changes may reflect two basically different causal mechanisms.

He and Singh (2020) also found a close association between the coseismic change of groundwater temperature and the coseismic change of groundwater level in some wells where both measurements are available (Fig. 8.3). Because temperature increases with depth, groundwater flows from a conductive fracture or aquifer into

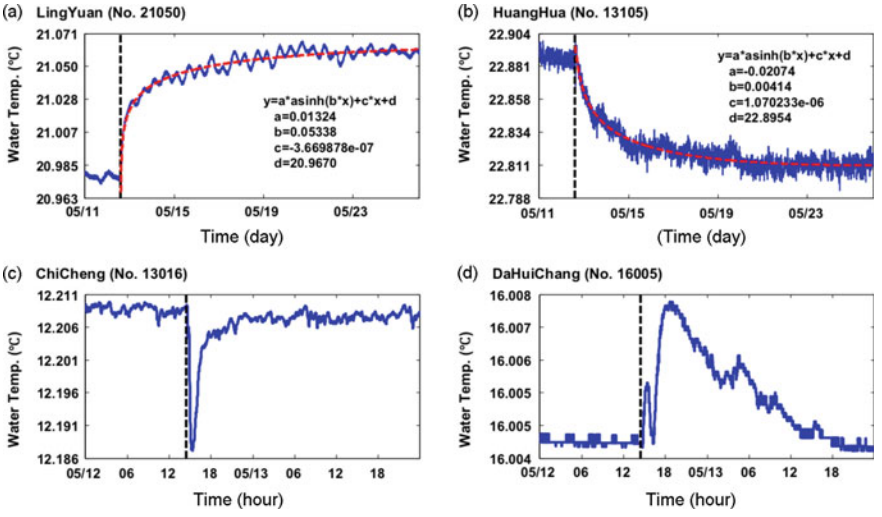

Fig. 8.2 Four types of coseismic groundwater temperature response to the Wenchuan earthquake. **a** Sustained temperature rise after the earthquake. **b** Sustained temperature fall after the earthquake. **c** Transient coseismic fall that recovers shortly afterwards. **d** Transient coseismic rise that recovers shortly afterwards (modified from He and Singh 2020)

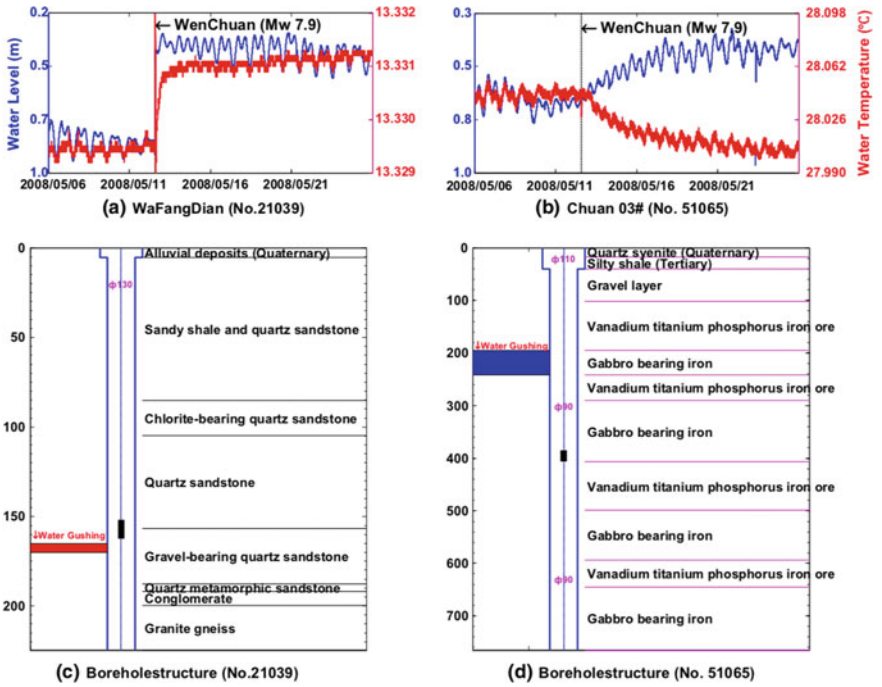

Fig. 8.3 **a** Sustained coseismic response of groundwater level and temperature in the same direction. **b** Sustained coseismic response of groundwater level and temperature in the opposite directions. **c** and **d** Lithology well logs of the two wells. Also shown are the relative positions of the temperature gauges (filled rectangles) and the conductive fractures (colored) in the wells (from He and Singh 2020)

the well will have a higher temperature than that at the temperature gauge if the hydraulically conductive fracture or aquifer is located deeper than the gauge, and vice versa. On the other hand, the relative locations of the temperature gauge in the well and the hydraulically conductive fracture or aquifer is unknown in most wells; thus either a temperature rise or a temperature fall is likely, which is consistent with the apparent random spatial distribution of the coseismic change of groundwater temperature after the Wenchuan earthquake (Fig. 8.1a).

While the hypothesis explains the sustained temperature changes (e.g., Fig. 8.2a, b), it may not be easily applied to explain the transient temperature changes (e.g., Fig. 8.2c, d); more discussion of the transient temperature changes is given in Sect. 8.6. Interpretation of these coseismic changes of groundwater temperature are made more challenging because of the lack of the lithology logs of the wells. Testing of different hypotheses on the causal mechanisms requires, in addition to accurate measurements of groundwater temperature and water level, accurate logs of the lithology and the locations of the conductive fractures and/or formations.

8.2.2 *Japan*

Miyakoshi et al. (2020) measured temperature–depth profiles in 10 wells distributed from the Aso Mountains to the lowlands after the 2016 Mw7.0 Kumamoto earthquake (Fig. 8.4), starting January 2017, nine months after the earthquake, until February 2018 when temperature stopped changing. Near the foot of the western Aso Mountain and the Takuma Plateau, groundwater temperature at depths >80 m first decreased and then increased (wells 1 and 3); at lower elevations, groundwater temperature generally showed a long-term warming. Also interesting to note is that this warming also occurs in the wells near the Suzenji fault zone (i.e., wells 6, 7 and 9) where significant groundwater drawdown over a 160 km^2 area was documented (Hosono et al. 2019).

The transient cooling in the well water at the foot of the Aso Caldera and the Takuma Plateau (Fig. 8.4a) was attributed to the post-seismic release of mountain groundwater (Miyakoshi et al. 2020), similar to the explanation of the post-seismic temperature decrease over the upper rim of an alluvial fan near the epicenter of the 1999 Chi-Chi earthquake (Sect. 8.3; Wang et al. 2012).

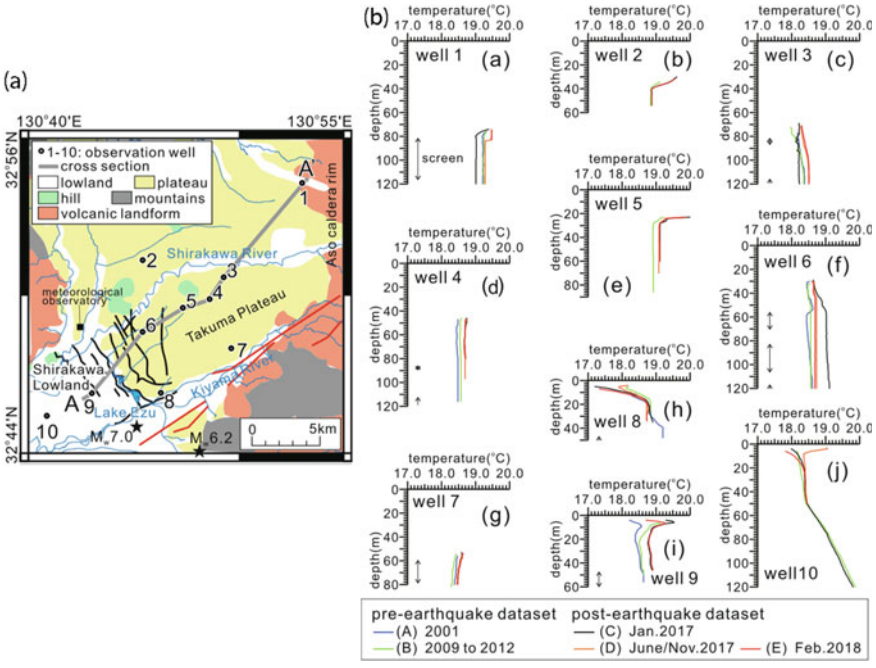

Fig. 8.4 **a** Map showing the study area and the distribution of wells from the western rim of the Aso Caldera (upper right) to the lowland (lower left). The NW-SE trending black lines show the location of the Suzenji fault zone. The well numbers correspond to those shown in (**b**). **b** Repeated temperature profiles in the wells shown in (**a**) before and after the 2016 Kumamoto earthquake (from Miyakoshi et al. 2020)

Miyakoshi et al. (2020) also proposed that the gradual warming of well water in the lowlands represents a long-term subsurface warming across the study area. An alternative interpretation of the gradual warming of groundwater in the lowland after the earthquake is enhanced basin-wide groundwater flow, as explained in Sect. 8.4, which has an upward component in the discharge area. This upward flow transports heat from greater depth, warming the groundwater at shallower depth, as explained in Sect. 8.3 (Wang et al. 2013).

8.2.3 Korea

A Mw5.8 earthquake occurred on 12 September 2016 near the city of Gyeongju, SE South Korea, the largest event in Korea recorded by modern instrumentation. Following the earthquake, changes of groundwater level, temperature and electrical conductivity were documented in a well 241 km to the west of the epicenter near the western coast of Korea (Lee et al. 2020). Temperature and electrical conductivity in this well were measured using an Eikelkamp diver (https://diver-water-level-logger.com/diver-water-level-loggers/ctd-diver.html) with an accuracy of ±0.1 °C and a resolution of ±0.01 °C; the sensor was sampled every second and was lowered into the borehole at a speed of ~20 cm/s (Kyoochui Ha, personal communication). Before the earthquake, the groundwater temperature above 50 m depth was sensitive to changes of surface temperature (Fig. 8.5), but below 50 m it became stable and showed a steady increase with depth, reflecting the local geothermal gradient. Following the earthquake, the groundwater temperature (red profile, Fig. 8.5) became evidently cooler below 50 m. The authors interpret this change to reflect an influx of cooler groundwater to the well through reactivated fracture paths; they also suggested that the influx of cooler groundwater was short lived because the temperature profile below 50 m recovered to the pre-earthquake profile about a month after the earthquake (black profile, Fig. 8.5).

An alternate explanation for the coseismic change of water temperature is that the water column in the well with the initial temperature is mechanically unstable and undergoes turbulent mixing when it is disturbed by the passing seismic waves, resulting in a water column more uniform in temperature (red curve in Fig. 8.5). Temperature recovered when the well water re-establishes thermal equilibrium with the wall rocks (blue curve in Fig. 8.5). Further discussion of this mechanism is given in Sect. 8.6.

8.3 Basin-Wide Changes

Groundwater flow has long been recognized as an effective means to promote heat transport across sedimentary basins (e.g., Forster and Smith 1989; Garven et al. 1993). As discussed in the last chapter, large earthquakes often release a large amount

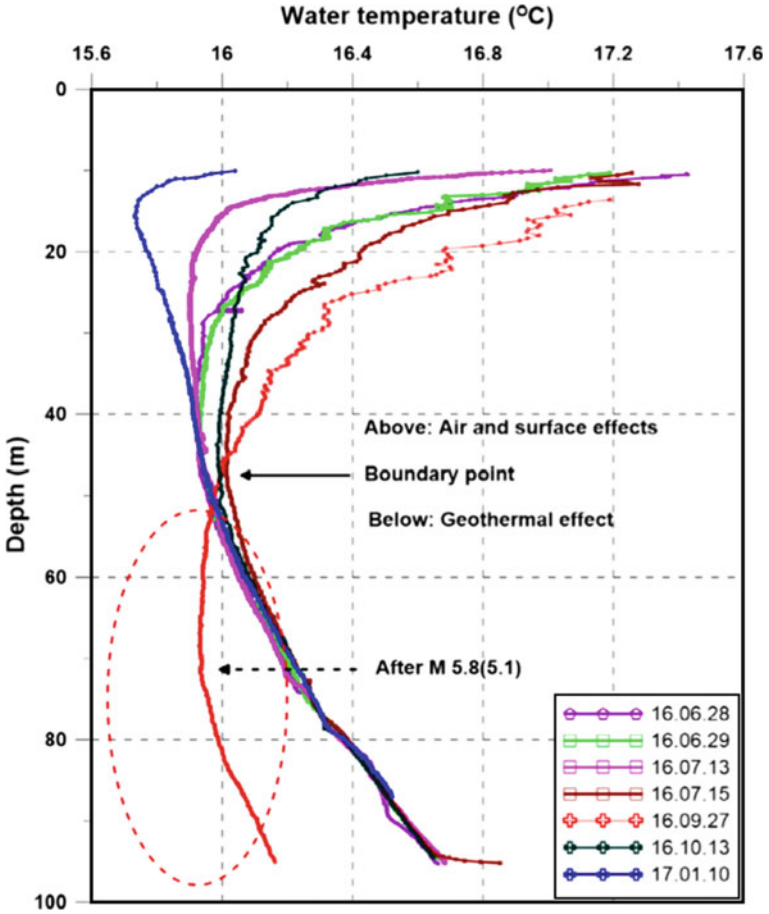

Fig. 8.5 Profiles of groundwater temperature in a well before and after the Mw5.8 Gyeongju earthquake. Dates for the profiles are shown in the legend. The dashed oval shows the lowering of the groundwater temperature after the earthquake (from Lee et al. 2020). The numbers in the legend show the time of measuremnt in year-month-date. For example: 16.09.27 means 2016, September 27.

of groundwater from mountains to nearby basins (e.g., Wang et al. 2004; Hosono et al. 2019). It should not be surprising that earthquakes might also cause basin wide change of groundwater temperature.

Figure 8.6 shows the epicenter of the Chi-Chi earthquake and a nearby alluvial fan on which groundwater temperature was measured in many wells before and after the earthquake. Because the geometry of this drainage basin is relatively simple and its hydrogeology is well understood through abundant borehole logging, the basin is ideal for revealing any regional pattern in the earthquake-induced temperature changes in groundwater and the causal hydrogeological processes.

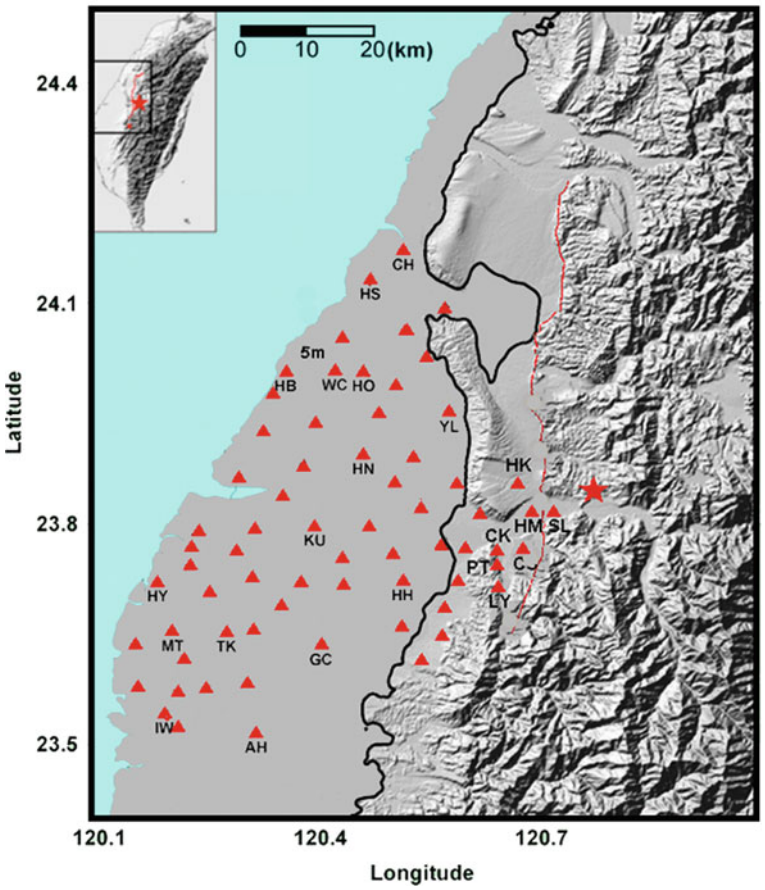

Fig. 8.6 Groundwater monitoring stations (red triangles) on an alluvial fan near the 1999 M7.6 Chi-Chi earthquake (red star) in Taiwan. Wells labeled with letters have temperature measurements before and after the 1999 Chi-Chi earthquake. Dashed curve shows the surface trace of the ruptured fault; solid black curve shows the thrust front of the Taiwan mountain belt; inset shows the location of the study area in Taiwan

Measurements were made in the wells during routine well maintenance, 7 months before and 2–3 months after the earthquake, using a temperature gauge with accuracy of ±0.1 °C. The measured groundwater temperatures before the Chi-Chi earthquake are projected onto an east-to-west profile as a function of distance from the surface trace of the NS-trending, ruptured fault on the east of the profile to the coast on the west. Scatter in the data (Fig. 8.7a) is partly due to superposition of data from different latitudes onto a single profile. In spite of the scatter, the data show a clear trend of increasing temperature from the foothills on the east to the coast on the west, indicative of active heat transport by groundwater flow from the upper rim of the alluvial fan across the basin to the coast. Figure 8.7b shows groundwater temperatures

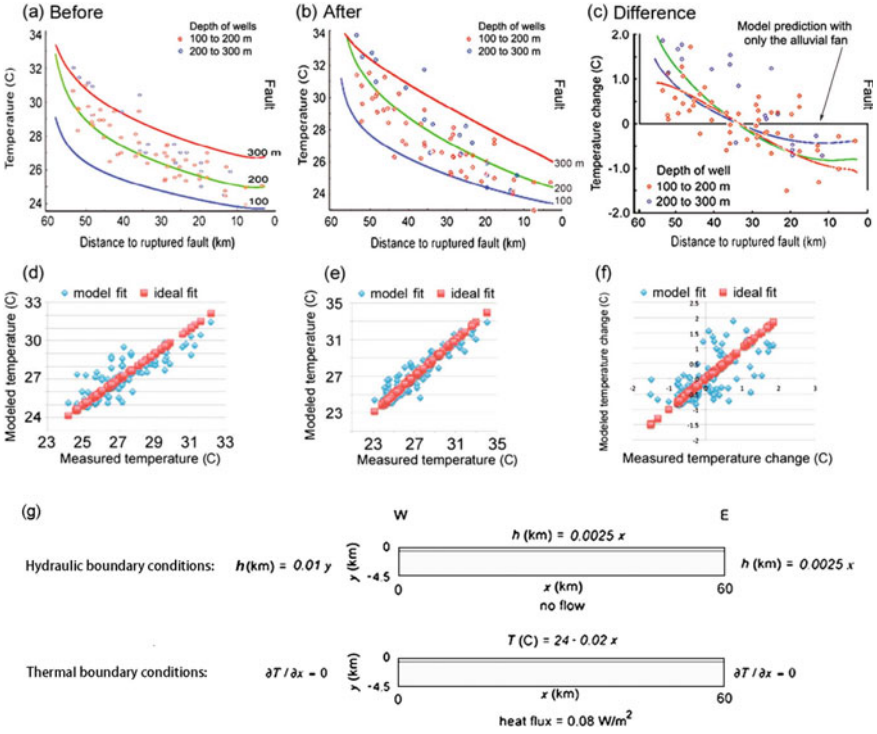

Fig. 8.7 **a** Groundwater temperature in wells on the Choshui alluvial fan ~7 months before the Chi-Chi earthquake. Circles are observed temperatures; different colors show measurements made at different depths. Note that numbering on the horizontal axis is from 60 km to 0 because distance is measured from the ruptured fault (indicated by the word "fault" on the right side of figure). **b** Groundwater temperature in the same wells 2–3 months after the earthquake. Circles are measured temperatures and curves are simulated temperatures 2–3 months after the earthquake. **c** Changes in groundwater temperature, i.e., difference between (**b**) and (**a**). Curves of blue, green and red colors in each diagram show, respectively, simulated groundwater temperatures before the earthquake at 100, 200, and 300 m below the surface. **d** and **e** Simulated temperatures plotted against measured temperatures before and after the earthquake, respectively. **f** Differences between the simulated temperatures before and after the earthquake plotted against the differences between the measured temperatures. **g** Hydrogeology model and boundary conditions used in simulating the groundwater flow and temperatures in (**a**), (**b**) and (**c**). The heat flux boundary condition at the base of the model is based on measured heat flux from deep exploration wells in the same area (Hwang and Wang 1993) (from Wang et al. 2013)

in the same wells 2–3 months after the Chi-Chi earthquake. Here temperatures show the same trend as that before the earthquake but temperatures are slightly lowered near the ruptured fault and raised near the coast relative to those before the earthquake. Figure 8.7c shows the difference between Fig. 8.7a, b, i.e., the *change* of temperature after the earthquake. Despite of the scatter, the data show a clear trend from negative differences (temperature decreases) near the eastern rim of the fan near the ruptured fault to positive differences (temperature increases) near the coast on the west.

Wang et al. (2013) attributed the observed changes in groundwater temperature to a basin-wide increase of groundwater flux after the earthquake. To test this hypothesis, they used an idealized 2-dimensional model (Fig. 8.7g) that extends sub-horizontally from the ruptured fault on the east to the coast on the west, and vertically down from the surface to a depth of ~4.5 km. The model parameters are based on the existing well tests and known hydrogeology of the area. The upper 0.5 km of the model represents the Holocene alluvial deposits, and the lower 4 km represents the Plio-Pleistocene conglomerates, and the lower boundary represents the top of the impervious Miocene shale. Water properties are taken as functions of temperature to account for the temperature effects on water density and viscosity that, in turn, affect the velocity and direction of groundwater flow. As shown in Sect. 2.5.2, the differential equations that control groundwater flow and heat transport in such situation are coupled and nonlinear. Numerical procedures are required to obtain a solution. Together with reasonable material properties (e.g., Tyan et al. 1996) and boundary conditions (Fig. 8.7g), Wang et al. (2013) used a finite-element method to simulate the temperatures as shown in colored curves in Fig. 8.7a, b and c. The reasonable agreement between the simulated and measured temperatures (Fig. 8.7d, e and f) lends support to the interpretation.

Another interesting result is the simulated temperature change with the assumption that groundwater flow is restricted to the alluvial fan (black line in Fig. 8.7c). The model result is significantly different from the observation, which suggests that a substantial portion of the earthquake-induced groundwater flow occurs deep beneath the alluvial fan and that large earthquakes may enhance permeability and thus basin-wide groundwater flow to depths of several km.

8.4 Springs

8.4.1 Cold Springs

Koizumi et al. (2019) surveyed 11 springs in the region that experienced strong ground motion during the 2016 Kumamoto earthquake (Fig. 8.8a) and sampled at intervals of a few weeks to several months. Fortunately, 8 of the 11 springs were also surveyed 1 month to a few years before earthquake. The results show no clear evidence of earthquake-related change to the spring temperature (Fig. 8.8b), even though the flow rate did show coseismic changes (increases at three springs e, g and k, decreases at f and h, and no change at the rest). This led the authors to suggest that there was little contribution in the enhanced flow from hydrothermal fluids. The conclusion seems to be supported by their measurement of the chemistry of the spring water as discussed in the next chapter.

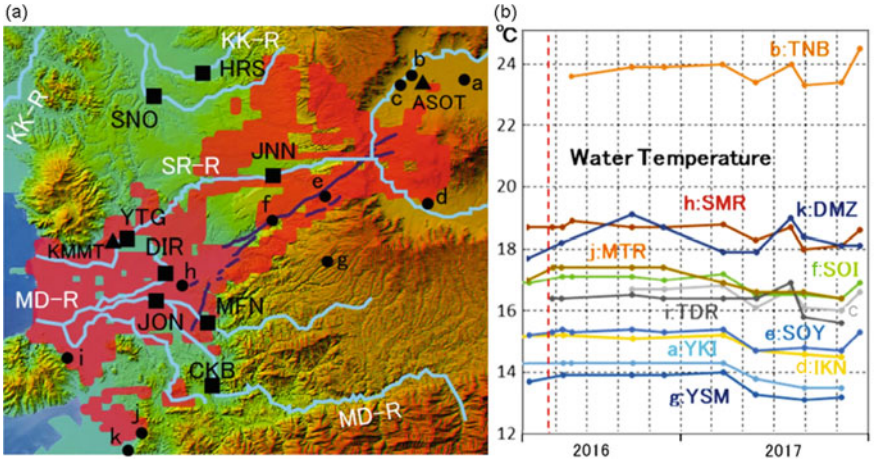

Fig. 8.8 Spring water temperature in central Kyushu. **a** Map showing the study area and the locations of the studied springs (black circles with labels). Area colored red experienced strong ground motion during the 2016 Kumamoto earthquake. **b** Time series of temperature of the studied springs in (**a**). No obvious change was recorded after the 2016 Kumamoto earthquake (marked by the red vertical dash line) (modified from Koizumi et al. 2019)

8.4.2 Hot Springs

One example of earthquake-induced change of hot spring temperature is from the Usami Hot Springs on the northeast coast of the Izu Peninsula in central Honshu, Japan. The term 'hot spring' is used following the preference by the authors (Mogi et al., 1989) even though measurements were made in a 600 m deep well installed in one of the springs. Accurate and continuous measurements of water temperature were made since 1982 (Mogi et al. 1989). Since 1985, however, the hot water in this well ceased to spout. Four temperature probes were installed in the well, but only the topmost probe's data were reported (Mogi et al. 1989). Figure 8.9a shows that, when there are no earthquakes, the temperature of the well water falls gradually with time; at the time of earthquakes, on the other hand, temperature rises first rapidly but then gradually to reach a peak temperature. Mogi et al. (1989) interpreted the gradual decline of temperature during normal times to indicate a decrease in the amount of geothermal water in the hot spring as a result of ongoing precipitation of obstacles in underground passageways, slowly blocking the flow of the geothermal water. When a fairly strong earthquake occurs, the seismic waves dislodge the obstacles, and the flow of the geothermal water suddenly increases and temperature suddenly rises. This mechanism is similar to that suggested for the enhanced permeability model proposed to explain the earthquake-induced sustained changes in groundwater level (Chap. 6) and increases in stream flow (Chap. 7).

Another example is the temperature response of the Copland hot spring, New Zealand, to the 2009 Mw7.8 Dusky Sound earthquake (15 July 2009) and the 2010

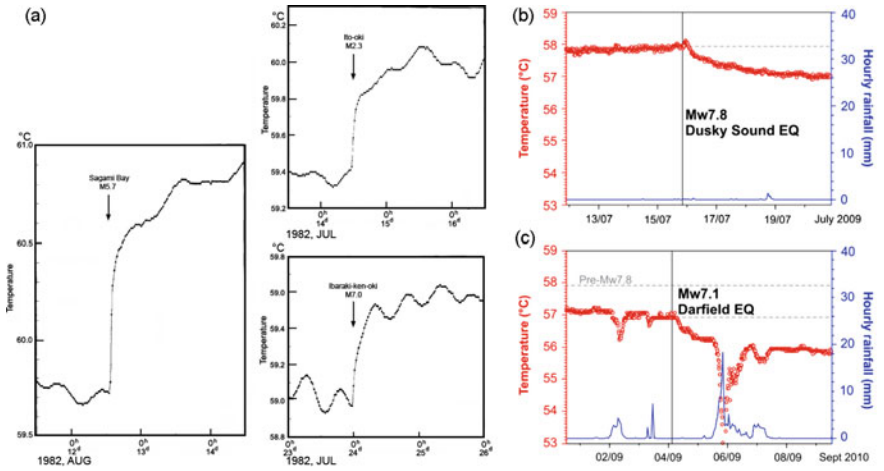

Fig. 8.9 **a** Examples of coseismic response of groundwater temperature in the Usami No. 24 well, Japan, to several earthquakes (from Mogi et al. 1989). Response of Copland spring temperatures (red) to the 2009 Mw7.8 Dusky Sound earthquake **b** and the 2010 Mw7.1 Darfield earthquake **c**; blue shows precipitation (from Cox et al. 2015)

Mw7.1 Darfield earthquake (Fig. 8.9b, c). The Copland hot spring is located in the foothills of the Southern Alp, about 12 km from the Alpine Fault. It has the strongest discharge among about forty thermal springs along the fault and emanates both water and gas at a temperature of ~57 °C through an alluvial fan deposit that overlies fractured metamorphic rocks (Cox et al. 2015). The earthquakes caused a ~1 °C delayed cooling over 5 days (Fig. 8.9b). The authors suggest that the delayed cooling was caused by an increased mixing of shallow-circulating meteoric water into the deep hot spring water after the earthquake, due perhaps to an increased infiltration of the shallow meteoric water through near-surface fractures generated by the earthquakes. The suggested mechanism seems to be consistent with the decreased concentrations of Cl, Li, B, Na, K, Sr and Ba and an increased SO_4 concentration in the spring water after the earthquakes.

Figure 8.10 plots the epicentral distance versus magnitude for earthquakes that caused water temperature changes in the Copland hot spring (Cox et al. 2015; red stars) and those within a radius of 600 km from the Usami No. 24 well that caused coseismic changes of water temperature in the thermal well (Mogi et al. 1989; red circles), together with those that caused other types of hydrological changes (King et al. 1994; Sato et al. 2000; Manga and Rowland 2009; Wang and Manga 2010a, b). Most responses of groundwater temperature occurred at an inferred seismic energy density between 10^{-2} and 10^{-1} J/m^3. Two responses to small earthquakes (M2 to 3) occurred at an inferred seismic energy density between 10^{-4} and 10^{-3} J/m^3. Mogi et al. (1989) interpreted the latter responses to represent a mix of foreshocks and earthquake swarms. Assuming that the data for hot springs in Fig. 8.10 are representative, the mechanism for changing hot spring and thermal well temperature

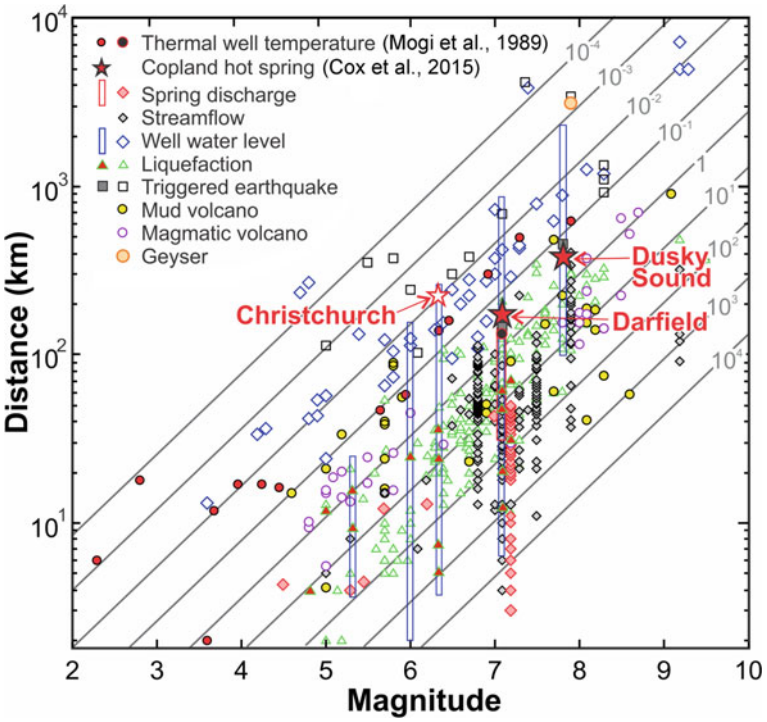

Fig. 8.10 Changes of temperature in some thermal wells in Japan in response to distant earthquakes (Mogi et al. 1989) and hot spring temperature change after the Mw7.8 Dusky Sound and Mw7.1 Darfield earthquakes at Copland hot spring (Cox et al. 2015), plotted on an earthquake magnitude versus distance diagram together with worldwide earthquake-triggered hydrological changes collated by Wang and Manga (2010a, b) with additions of spring discharge changes (King et al. 1994; Sato et al. 2000; Manga and Rowland 2009). The response of Copland spring following the Mw6.3 Christchurch earthquake is plotted for reference, although the response was not definitive (Cox et al. 2015). Contours of constant seismic energy density follow Wang and Manga (2010a, b) (modified from Cox et al. 2015)

requires a higher seismic energy density than that for changing groundwater level. The earthquakes for which changes were regarded as precursory (marked as ringed red circles; Mogi et al. 1989) will be discussed further in Chap. 13 on earthquake precursors.

8.5 Seafloor Measurements

8.5.1 Subduction Zones

Earthquake-induced temperature changes in subduction zones are important for understanding the mechanics of seismic hazards but are also difficult to measure. Part of the difficulty is the great depths of the seafloor in subduction zones. After the March 2011 Mw9.0 Tohoku-Oki earthquake off the Pacific coast of Japan, the Japan Trench Fast Drilling Project of the Integrated Ocean Drilling Program drilled a borehole (Fig. 8.11a) from the seafloor at a depth of 6.9 km below the mean sea level and reached the main plate boundary fault at a depth of ~820 m beneath the seafloor (mbsf). A string of 55 closely spaced temperature loggers with accuracy of 0.001 °C (Fig. 8.11b) was installed in the fully cased 20-cm borehole across the fault, and temperature measurements started 16 months after the earthquake (Fulton et al. 2013). The sensor string was recovered after 9-months of operation. The measurements captured a 0.31 °C temperature anomaly at the depth of the inferred plate boundary fault (Fig. 8.11b). At the same time, it also captured temperature increases at ~763 and 810 mbsf after a December 2012 Mw7.4 local earthquake but a temperature decrease at 784 mbsf (Fig. 8.11b). Fulton et al. (2013) interpreted the temperature anomaly at the depth of the inferred plate boundary fault to correspond to 27×10^6 J/m^2 of dissipated energy during the earthquake, implying a frictional coefficient of

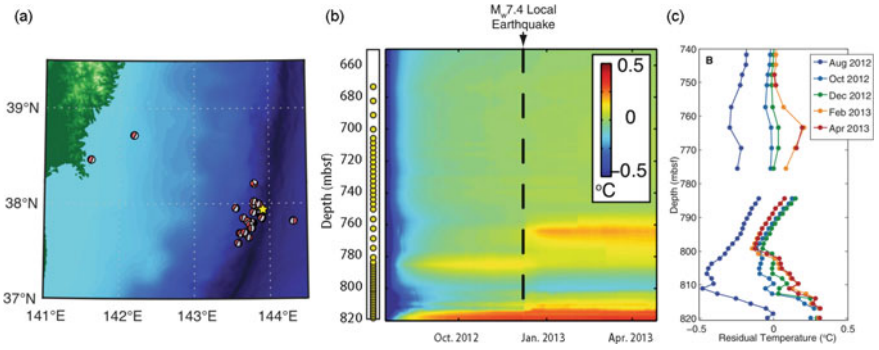

Fig. 8.11 **a** Map showing the site of the Japan Trench Fast (JFAST) Drilling Project (star). Focal mechanisms show regional earthquakes during the 9-month observation period (Fulton et al. 2013). **b** Residual daily average temperature after the background geotherm was removed. Yellow circles on the left edge of the diagram show sensor positions, and each row in the diagram represents the corresponding sensor's data. Each column is the daily average temperature after an average background geotherm is removed. The occurrence of a local Mw7.4 earthquake is shown by dashed line. Notice that after the earthquake, temperature increased at ~763 and ~810 mbsf but decreased at ~784 mbsf (Fulton and Brodsky 2016). **c** Depth profiles of residual temperature from five dates through the experiment separated by 2-month intervals (Fulton et al. 2013). Notice the different depth scales between (**b**) and (**c**). Relatively cool temperatures in August reflect the effects of drilling disturbance (modified from Fulton et al. 2013; Fulton and Brodsky 2016)

0.08, substantially smaller than the static friction for most rocks. This result implies a very low frictional resistance on the subduction fault, which is potentially important for understanding earthquake mechanics in subduction zones.

The interpretations by Fulton et al. (2013) and Fulton and Brodsky (2016) of the JFAST temperature measurement are interesting and provocative. Since pore pressure was not measured during the JFAST experiment, the interpretation of the temperature anomaly may be challenging. Fulton et al. (2013) interpreted the temperature anomaly at the inferred plate boundary fault (~820 mbsf) as the decaying signature of the frictional heat during the 2011 Tohoku-Oki earthquake and argued against the alternative interpretation of advection of heat by fluid flow up a permeable fault by stating that there was no indication of high permeability on the resistivity log at the depth of the inferred fault. On the other hand, they attributed the temperature increase at ~763 and 810 mbsf and the temperature decrease at 784 mbsf following the 2012 Mw7.4 local earthquake (Fig. 8.11b) to advection of heat by fluid flow.

Fulton and Brodsky (2016) further filtered out the long-wavelength signals in their record to highlight the remaining high-pass filtered fluctuations following the 2012 local earthquake in Fig. 8.12, which they attributed to fluid flow through the fault damage zone. The filtered temperature record at each depth is overlain on this diagram to highlight the patterns of temperature variation.

The changes on these temperature profiles were rapid, consistent with the hypothesis of advection of heat by flow. Fulton and Brodsky (2016) considered two candidates for the flow mechanism: coseismic influx of pore fluid from the formation to the borehole, and an internal flow entirely confined in the borehole, similar to that suggested by Shi et al. (2007). They favored the first mechanism and argued that these patterns are consistent with transient fluid flow from permeable pathways within the formation into the borehole annulus as illustrated by the schematic drawing on the

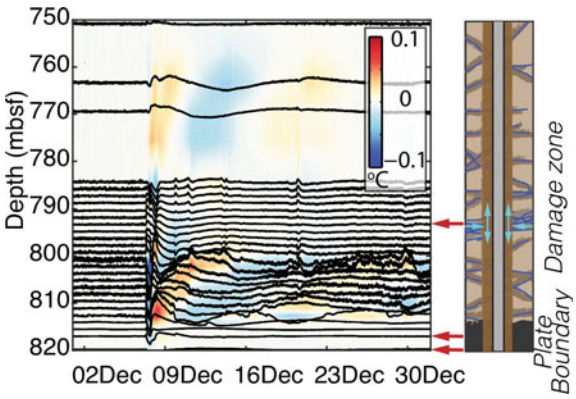

Fig. 8.12 High-pass filtered temperature data from depths 750–820 m below seafloor at the JFAST site during December 2012. Filtered temperature record at each depth is overlain to further highlight the temperature patterns. Cartoon illustrates how fluid flow out of a permeable zone results in flow up and down the borehole annulus (modified from Fulton and Brodsky 2016)

right of Fig. 8.12. Because the background geotherm increases with depth, this model predicts that fluids flowing into the borehole are warmer than the surroundings when they flow up the borehole and cooler than the surroundings when they flow down, resulting in the observed temperature pattern following the Mw7.4 event.

Fulton and Brodsky (2016) also cited several reasons to support their hypothesis that the variations on the high-pass filter profiles (Fig. 8.12) are caused by flows between some permeable formations and the well, rather than by flows confined in the borehole. They first argued that if fluid movement is internal to the borehole and independent of flows from the formation, then the effects should be observed at all depths, contradicted by signals that are repeatedly seen to center around the same depths over time. They then argued that, if a convection cell in the borehole was the cause, fluids would have to overturn over tens of meters within a borehole annulus with a radius of several centimeters, which is difficult. Finally, they argued that if water movement is confined solely within the borehole, the temperature change would have been greatest immediately after an earthquake, whereas the observed transient changes typically occurred over ~0.1 day.

These arguments can be contested. The first argument is based on the assumption of an initially uniform temperature gradient in the water column. The temperature gradient in the well is more likely to have perturbations due to fluid influxes through permeable fractures and formations. These perturbations may significantly influence the initiation of flow in different sections of the well. The second argument is based on the assumption that convection of well water occurs through laminar flow. Because the water column in wells with a geothermal temperature gradient is mechanically unstable (Sect. 8.6), it may undergo turbulent mixing when perturbed by passing seismic waves, as demonstrated by numerical simulations carried out by Shi et al. (2007); the results of the numerical simulations show that turbulent mixing easily occurs in a well with a geothermal gradient to quickly change the initial temperature. Their last argument was likely to be based on the theory of flow in a uniform borehole. Since the geometry of the real borehole is not uniform , water movement in the borehole and the associated temperature change may be complicated and require experimental or numerical evaluation. Observations in the Tangshan well (Sect. 8.6) show that the thermal effect of turbulent mixing in the well takes from 10 min to 2 h to reach the largest perturbations.

8.5.2 Near Oceanic Ridge

Several types of temperature changes near oceanic ridges have been documented. Some responded to earthquake swarms located directly below the vents (Sohn et al. 1998; Baker et al. 1999), some were responses to earthquakes along adjacent spreading centers (Dziak et al. 2003), and others were responses to ridge-flank earthquake swarms with epicenter distances up to 50 km away (Johnson et al. 2000, 2001).

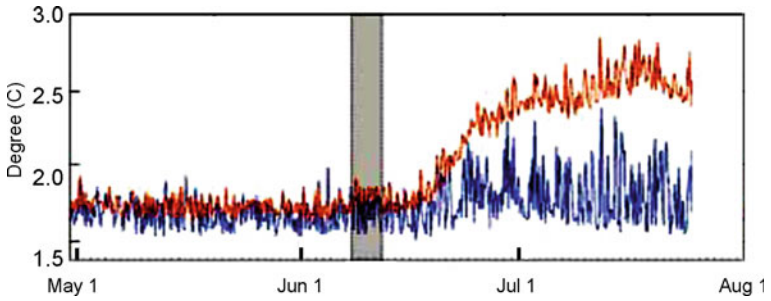

Fig. 8.13 Temperature records from a site on the Endeavour axial valley of the Juan de Fuca Ridge. The June 8–15, 1999, earthquake swarm is marked by the vertical shaded bar. Upper trace indicate data from thermistors located within the vents; blue trace indicate data from thermistors deployed in the adjacent (non-vent) bottom water (from Johnson et al. 2000)

Earthquake-induced changes of groundwater temperature near mid-oceanic ridges have been documented from hydrothermal veins and in ODP boreholes, which are discussed below in sequence. Temperature of hydrothermal vents along mid-oceanic ridges responded to local and distant earthquakes (Sohn et al. 1998, 1999; Johnson et al. 2000, 2001, 2006; Dziak et al. 2003). In the following we first discuss the results of some measurements in the vents along the Juan de Fuca Ridge in response to local and distant earthquake swarms.

On 8 June 1999, an earthquake swarm occurred beneath a segment of the ridge and lasted about a week (Johnson et al. 2001). A thermistor array, deployed before the earthquake swarm within a low temperature vent system on the Juan de Fuca Ridge, 7.5 km away from the earthquake swarm, recorded widespread increases of temperature. In Fig. 8.13 (Johnson et al. 2000), the gray band shows the occurrence of the earthquake swarm, the upper curve shows the temperature from a thermistor located directly in a vent, and the lower curve shows the temperature of the axial valley bottom water. The earthquake swarm produced a slow increase in vent temperature 8 days after the initiation of the swarm. All monitored vents within the axial valley responded similarly, with delayed responses varying from a few days to a month and the net heat flux increased by a factor of ten (Johnson et al. 2001).

Between 1–7 June 2000, another earthquake swarm, with 170 earthquakes and a mainshock of Mw6.2, occurred on the western Blanco Transform Fault. Two temperature probes, located in hydrothermal vents in an adjacent spreading center on the Juan de Fuca Ridge, ~39 km away from the earthquake swarm, registered temperature decreases, one occurring over days to weeks while the other changes were coseismic, as shown in the Fig. 8.14. The onset of the temperature decreases was gradual, but accelerated after the occurrence of the earthquake swarm, with a total decrease of more than 20 °C (Dziak et al. 2003). The fact that earthquakes can influence sub-surface hydrothermal fluids on the sea floor over significant distances from the epicenters, by either increasing or decreasing flow rates, implies that fluids in aquifers beneath the sea floor are frequently ‘stirred’ tectonically (Dziak et al. 2003).

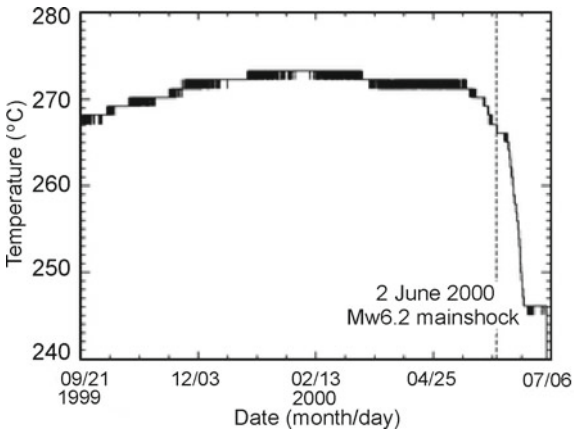

Fig. 8.14 During June 1–7, 2000, an earthquake swarm, with 170 earthquakes and a mainshock of Mw6.2 occurred on the western Blanco Transform Fault. Two temperature probes, located in the hydrothermal vent of an adjacent spreading center, ~39 km away from the earthquake swarm, registered temperature decreases of more than 20 °C. One of the records is shown in this figure (from Dziak et al. 2003)

Temperature changes at hydrothermal vents after earthquake swarms are often interpreted to be the result of opening of clogged cracks and fractures that enhance permeability and flow between reservoirs of different temperatures (e.g., Johnson et al. 2000; Dziak et al. 2003). The substantial delay between the onset of the temperature response and the earthquake swarms may represent the time required for fluids of different temperatures to pass through the newly opened channels and to warm the pathways through which the fluid flows.

Temperature probes, as well as pore-pressure probes, in ODP boreholes on the eastern flank of the Juan de Fuca Ridge, responded to the June 8, 1999 earthquake swarm on the ridge (Fig. 8.15 from Davis et al. 2001). Noteworthy is that, while the temperature probe registered changes coinciding not only with the first earthquake, but also with the later earthquakes in the swarm (Fig. 8.15b), the pressure probe registered only a transient change coinciding with the first earthquake (Fig. 8.15a). The coseismic temperature changes were always negative and the amplitudes of the later temperature transients generally reflect the magnitude of the earthquakes, with the greatest change nearly as large as the initial one.

This observation by Davis et al. (2001) in the ODP boreholes is particularly interesting because both pore pressure and temperature were measured in the same boreholes, allowing a more constrained interpretation of the data. As noted earlier, while pore pressure responded only to the first earthquake in the swarm, temperature in the same boreholes responded to many later earthquakes, in addition to the first one. An explanation for why pore pressure responded only to the first earthquake (Fig. 8.15a) may be offered based on the hypothesis that the enhanced permeability occurs when clogged fractures are cleared. According to this hypothesis, the recovery of the enhanced permeability requires the fluid passageways to be resealed by precipitates, which may take much longer time than the time between successive earthquakes in the swarm, and thus the local pressure sources may not have time to re-pressurize between the successive earthquakes. An explanation for why temperature responded not only to the first but also to the later earthquakes (Fig. 8.15b) may

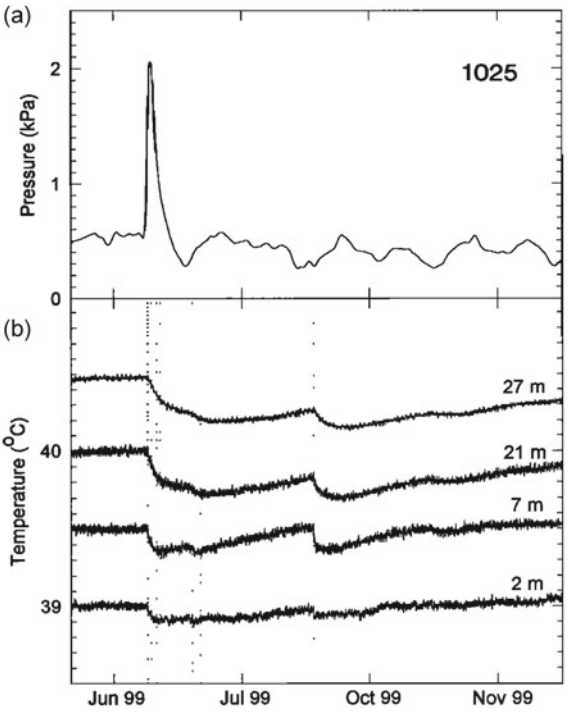

Fig. 8.15 Four-month record of **a** pore pressure and **b** temperatures in ODP borehole 1025C on the eastern flank of the Juan de Fuca Ridge. Times of the individual seismic events are indicated by dotted vertical lines. Depths of the temperature sensors are relative to the top of the basement. The uncased part of the hole extends a total of 47 m below the top of the basement. Temperature records are offset from the sensor at 21 m by 0.5 K for plotting convenience (from Davis et al. 2001)

be offered by using the model of turbulent mixing in wells (Shi et al. 2007; Sect. 8.6). After the water in the borehole becomes still, the water column readily re-establishes thermal equilibrium with the wall rocks , resetting the mechanical instability in the water column required for turbulent mixing before the next seismic event. Thus the water column may repeatedly undergo turbulent mixing when perturbed by earthquakes, causing recurrent temperature changes in the well water (see Sect. 8.6 for more detail).

8.6 Turbulent Mixing of Well Water

As shown in this chapter, most existing studies invoked an earthquake-enhanced permeability to interpret earthquake-induced changes of groundwater temperature. A less well known, but potentially common, process is a turbulent mixing of water in a well when the water column is disturbed by seismic waves (Shi et al. 2007). Since this mechanism has been invoked several times in this chapter to explain coseismic changes of groundwater temperature (e.g., Sections 8.2.3, 8.5.1, 8.5.2), we discuss this process here with its observational and physical basis.

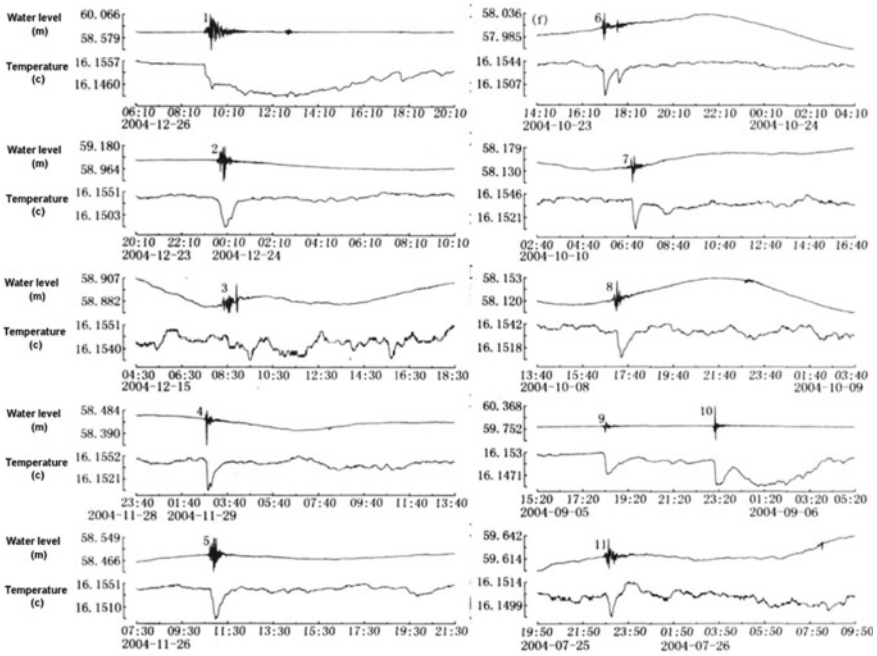

Fig. 8.16 Diagrams **a–j** show changes in temperature and groundwater level documented simultaneously in a well in the city of Tangshan, China, during 12 earthquakes. For each earthquake, the upper trace shows oscillations in groundwater level and the lower trace shows temperature changes. Note that some traces contain two earthquakes (from Shi et al. 2007)

Simultaneous and continuous measurements of temperature and groundwater level have been carried out in a well in the city of Tangshan, China, since 2001, together with the documentation of seismic waves by a seismometer installed near the well. Temperature was measured with a high-resolution (10^{-4} °C) probe 125 m beneath the wellhead. Figure 8.16 shows the hydroseismograms and concurrent temperature changes during 12 earthquakes (note that some traces contain two earthquakes). It is interesting that, in response to all the documented earthquakes, water level in this well oscillates (hydroseismogram; Fig. 8.16) and temperature always drops independent of the orientation of the causal fault, the distance from the hypocenter, and the magnitude of the seismic events. The rate of temperature drop is generally rapid: it begins when the seismic waves arrive, and the well-water oscillates with amplitudes ranging from several centimeters to ~1 m. Temperature decreases by 0.001 to 0.01 °C and generally takes 10–20 min to 2 h to reach the minimum. The recovery process takes 1 to ~10 h.

The observation that well water temperature always drops during the passage of the seismic waves from distant earthquakes with different mechanisms and fault orientations rules out static strain as a possible mechanism. Since the *average* velocity and displacement during the water-level oscillations are zero (Fig. 8.16), there is no

net transport of heat due to advection. Shi et al. (2007) suggested that the observed decrease of well water temperature was due to turbulent mixing of the water column in the well. Under static conditions, the temperature in the water column readily equilibrates with the local geotherm by conductive heat exchange with the wall rocks. Since the compressibility of water is relatively small, the change of density in static well water is controlled by thermal expansion. Density of the water column therefore decreases with depth, resulting in a state of mechanical disequilibrium. Hence, when the water column is disturbed by seismic waves, it may undergo turbulent mixing to reach a state of uniform temperature and density. To support the turbulent mixing model, Shi et al (2007) simulated the earthquake-induced turbulent heat transfer in the Tangshan well using finite element modeling, a formulation for turbulent heat flux according to a generalized Fick's law (Pinson et al. 2007), and a simplified differential equation for the statistically averaged temperature (Shi et al. 2007)

$$\frac{\partial T}{\partial t} = D\frac{\partial^2 T}{\partial z^2},$$

where D is a generalized thermal diffusivity and is the sum of a static thermal diffusivity and a turbulent thermal diffusivity. Solving the system of equations requires the knowledge of velocity and turbulent diffusivity profiles. Since neither of these are known, Shi et al (2007) greatly simplified the problem with assumed D values. They also used the local geotherm for the initial temperature and various boundary conditions to broadly cover the range of possibilities. Figure 8.17 shows one of the simulated temperature profiles in the well as a function of time; in this simulation, where the turbulent thermal diffusivity are assumed to be a constant of 1 m^2/s, and the top and the base of the water column is assumed to be thermally insulated. The latter assumption may be justified by the relatively short duration of the temperature change (Fig. 8.16), the relatively low thermal conductivity of rocks and air, and the small heat capacity of air.

Even though the simulation of the turbulent heat transfer process may be simplified, the results still provide a qualitative understanding of the process. It shows that turbulent mixing in the water column causes its temperature gradient and thus its mechanical instability to quickly decrease with time. After the water becomes still, however, thermal conduction between the water column and the wall rocks becomes the dominant heat exchange process, which readily re-establishes the geothermal gradient and re-instates the mechanical disequilibrium in the water column.

The mixing model may be further supported by a recent study of the temperature change in a well after the 2016 Mw5.8 Gyeongju earthquake in Korea (Sect. 8.2.3; Lee et al. 2020). As Fig. 8.5 shows, before the earthquake, temperature of the water column in this well at depths >50 m conformed to the local geothermal gradient. This is because that the skin depth of the annual surface fluctuation of temperature is ~50 m and the temperature at depths below 50 m usually has the geothermal gradient. As explained in Sect. 8.2.3, this temperature gradient implies a decrease

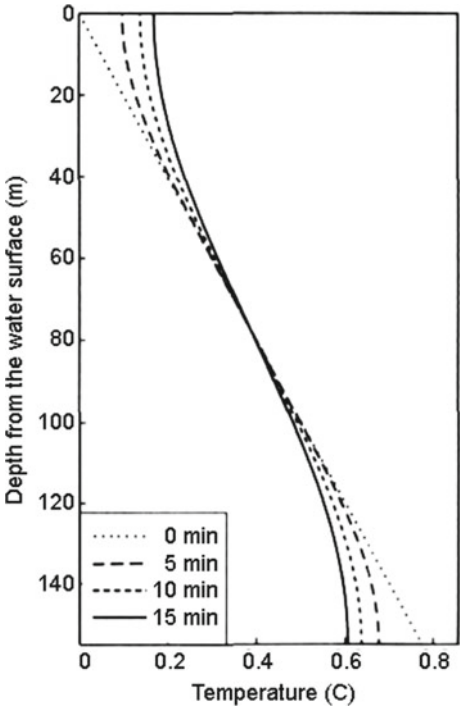

Fig. 8.17 Simulated temperature profiles with depth at four distinct times. The simulation assumed a constant turbulent thermal diffusivity of 1 m^2/s, an initial temperature equal to the local geotherm (adjusted to zero at the top), and thermal insulation at the top and the bottom of the water column (from Shi et al. 2007)

of density with depth and thus a state of mechanical disequilibrium in the water column. Soon after the earthquake, temperature in the well (red curve in Fig. 8.5) became nearly uniform with depth, reflecting a change of density distribution from a mechanically unstable state to a mechanically stable state, and this rapid change can only occur by turbulent mixing of the initially thermally stratified water column. After the earthquake, temperature in the well recovered to the geothermal gradient (black curve in Fig. 8.5), re-instating the mechanical disequilibrium.

Observations (Figs. 8.5, 8.15b and 8.16) thus suggest that turbulent mixing of well water may commonly occur when the water column is disturbed by seismic waves. Such temperature changes are relatively large and may last from an hour (Fig. 8.16) to a month (Figs. 8.5, 8.15b). Such changes may easily mask the more subtle changes due to geological processes such as frictional heat on ruptured faults during earthquakes and should be carefully removed in order to retrieve the signals produced by hydrogeological processes.

Since the temperature in the Tangshan well was measured at a single depth, it may not provide sufficient constraints on the model. Shi et al. (2007) proposed that the hypothesis could be tested by installing a string of high-resolution temperature probes at selected depths in the well to better constrain the model. Such measurements, though not done in this well, were realized in the borehole drilled to the ruptured fault after the 2011 Mw9.0 Tohoku-Oki earthquake off the Pacific coast of Japan, as discussed in Sect. 8.5.1.

8.7 Concluding Remarks

As noted, progress in understanding earthquake-induced changes of groundwater temperature has been slow, largely because relevant quantitative data are relatively scarce and instrumental measurements of earthquake-induced temperature changes started only in the last two decades. On the other hand, the available observations have provided highly valuable information for constraining models of earthquake-induced groundwater flow. Most changes of temperature in hot springs and submarine hydrothermal vents can be explained by a model of earthquake-enhanced permeability that is due to the dislodging of precipitates from clogged fluid channels, such as pre-existing fractures. Unclogged fractures act to breach hydrologic barriers (such as aquitards) and to connect otherwise isolated aquifers or other fluid sources.

Another complication for understanding the geological implications of the measured groundwater temperature is that the measured temperature may be strongly affected by local factors such as the coseismic influx of groundwater into the well through hydraulically conductive fractures and formations (He and Singh 2020). Since such local factors may strong affect the measured temperature to mask the more subtle changes due to other physical processes such as rock friction, it can be challenging to interpret specific measurements without a priori knowledge about the locations of the conductive fractures in the well. Hence measurement of water flow and logging of conductive fractures/formations in the well may be important to constrain the interpretations of measured groundwater temperature.

Since the water column in thermal equilibrium with the local geothermal temperature is often in a state of mechanical disequilibrium, turbulent flow may occur in the well when the water column is disturbed by seismic waves. Such mixing of water may obscure the more subtle signals from geological processes. While the details of the model may require further quantification, it nonetheless shows that the effect of turbulent mixing of well water should be carefully considered when interpreting observed temperature changes to understand hydrogeological processes.

Earthquake-induced changes in temperature of groundwater contain rich information about the subsurface hydrogeological processes. This information has been relatively less developed and much remains to be explored and learned. With the advances in instrumental technology, data management, analysis and interpretation, it may be timely to measure groundwater temperature routinely in field programs.

References

Baker ET, Fox CG, Cowen JP (1999) In situ observations of the onset of hydrothermal discharge during the 1998 submarine eruption of Axial volcano, Juan de Fuca Ridge. Geophys Res Lett 26:3445–3448

Cox SC, Menzies CD, Sutherland R et al (2015) Changes in hot spring temperature and hydrogeology of the Alpine Fault hanging wall, New Zealand, induced by distal South Island earthquakes. Geofluids 15:216–239. https://doi.org/10.1111/gfl.12093

Davis EE, Wang K, Thomson RE et al (2001) An episode of seafloor spreading and associated plate deformation inferred from crustal fluid pressure transients. J Geophy Res 106:21953–21963
Dziak RP, Chadwick WW, Fox CG et al (2003) Hydrothermal temperature changes at the southern Juan de Fuca Ridge associated with M-w 6.2 Blanc transform earthquake. Geology 31:119–122
Forster C, Smith L (1989) The influence of groundwater flow on thermal regime in mountainous terrain: a model study. J Geophys Res 97:9439–9451
Fulton PM, Brodsky EE, Kano Y et al (2013) Low coseismic friction on the Tohoku-Oki fault determined from temperature measurements. Science 342:1214–1217. https://doi.org/10.1126/science.1243641
Fulton PM, Brodsky EE (2016) In situ observations of earthquake-driven fluid pulses within the Japan Trench plate boundary fault zone. Geology 44:851–854
Garven G, Ge S, Person MA et al (1993) Genesis of stratabound ore deposits in the midcontinent basins of North America. 1. The role of regional groundwater flow. Am J Sci 293:497–568
He A, Singh RP (2019) Groundwater level response to the Wenchuan earthquake of May 2008, Geomatics. Nat Hazards Risk 10:336–352. https://doi.org/10.1080/19475705.2018
He A, Singh RP (2020) Coseismic groundwater temperature response associated with the Wenchuan earthquake. Pure Appl Geophys 177:109–120
Hosono T, Yamada C, Shibata T et al (2019) Coseismic groundwater drawdown along crustal ruptures during the 2016 Mw 7.0 Kumamoto earthquake. Water Resour Res 55:5891–5903. https://doi.org/10.1029/2019WR024871
Hwang WT, Wang C-Y (1993) Sequential thrusting model for mountain building: constraints from geology and heat flow from Taiwan. J Geophys Res 98:9963–9973. https://doi.org/10.1029/92JB02861
Johnson HP, Hutnak M, Dziak RP et al (2000) Earthquake-induced changes in a hydrothermal system on the Juan de Fuca mid-ocean ridge. Nature 407:174–177
Johnson HP, Dziak RP, Fisher CR et al (2001) Impact of earthquakes on hydrothermal systems may be far reaching. EOS Trans Am Geophys Union 82:233–236
Johnson HP, Baross JA, Bjorklund TA (2006) On sampling the upper crustal reservoir of the NE Pacific Ocean. Geofluid 6:251–271
King CY, Basler D, Presser TS et al (1994) In search of earthquake-related chemical changes along the Hayward fault. Appl Geochem 9:83–91
Koizumi N, Minote S, Tanaka T et al (2019) Hydrological changes after the 2016 Kumamoto earthquake, Japan. Earth Planet Space 71:128. https://doi.org/10.1186/s40623-019-1110-y
Lee SH, Lee JM, Yoon H et al (2020) Groundwater impacts from the M5.8 earthquake in Korea as determined by integrated monitoring systems. Groundwater. https://doi.org/10.1111/gwat.12993
Ma Z, Fu Z, Zhang Y et al (1990) Earthquake prediction: nine major earthquakes in China (1966–1976). Seismological Press, Beijing, p 332 (in Chinese)
Manga M, Rowland JC (2009) Response of Alum Rock springs to the October 30, 2007 Alum Rock earthquake and implications for the origin of increased discharge after earthquakes. Geofluids 9:237–250
Manga M, Beresnev I, Brodsky EE et al (2012) Changes in permeability caused by transient stresses: field observations, experiments, and mechanisms. Rev Geophys 50:RG2004
Miyakoshi A, Taniguchi M, Ide K et al (2020) Identification of changes in subsurface temperature and groundwater flow after the 2016 Kumamoto earthquake using long-term well temperature-depth profiles. J Hydrol 582. https://doi.org/10.1016/j.jhydrol.2019.124530
Mogi K, Mochizuki H, Kurokawa Y (1989) Temperature changes in an artesian spring at Usami in the Izu Peninsula (Japan) and their relation to earthquakes. Tectonophysics 159:95–108
Pinson F, Gregoire O, Quintard M et al (2007) Modeling of turbulent heat transfer and thermal dispersion for flows in flat plate heat exchangers. Int J Heat Mass Transf 50:1500–1515
Sato T, Sakai R, Furuya K et al (2000) Coseismic spring flow changes associated with the 1995 Kobe earthquake. Geophys Res Lett 27:1219–1222
Shi Y, Cao J, Ma L et al (2007) Teleseismic coseismic well temperature changes and their interpretation. Acta Seismol Sin 29:265–273 (in Chinese with English abstract)

Sohn RA, Fornari DJ, Von Damm KL et al (1998) Seismic and hydrothermal evidence of a cracking event on the East Pacific Rise near 98509N. Nature 396:159–161
Sohn RA, Hildebrand JA, Webb SC (1999) A microearthquake survey of the high-temperature vent fields on the volcanically active East Pacific Rise (98 509 N). J Geophys Res 104:25367–25378
Tyan CL, Chang YM, Lin WK et al (1996) The brief introduction to the groundwater hydrology of Choshui River Alluvial fan. In: Conference on groundwater and hydrology of the Choshui River Alluvial Fan, Taiwan. Water Resources Bureau 207–221 (in Chinese)
Wang CY, Wang CH, Manga M (2004) Coseismic release of water from mountains: evidence from the 1999 (Mw = 7.5) Chi-Chi, Taiwan, earthquake. Geology 32:769–772
Wang CY, Manga M (2010a) Earthquakes and water. Lect Notes Earth Sci 114:235
Wang CY, Manga M (2010b) Hydrologic responses to earthquakes and a general metric. Geofluids 10:206–216
Wang CY, Manga M, Wang CH, Chen CH (2012) Earthquakes and subsurface temperature changes near an active mountain front. Geology 40:119–122
Wang CY, Wang LP, Manga M, Wang CH (2013) Basin-scale transport of heat and fluid induced by earthquakes. Geophys Res Lett 40:3893–3897. https://doi.org/10.1002/grl.50738